Carbohydrate Polymers 117 (2015) 443–451

Contents lists available at ScienceDirect

Carbohydrate Polymers

journal homepage: www.elsevier.com/locate/carbpol

Cellulose nanocrystals' production in near theoretical yields by 1-butyl-3-methylimidazolium hydrogen sulfate ([Bmim]HSO_4) – mediated hydrolysis

Jia Mao[a,b], Barbara Heck[c], Günter Reiter[b,c], Marie-Pierre Laborie[a,b,*]

[a] Chair of Forest Biomaterials, Faculty of Environment and Natural Resources, Albert-Ludwig-University of Freiburg, Werthmannstr. 6, 79085 Freiburg, Germany
[b] Freiburg Materials Research Center (FMF), Albert-Ludwig-University of Freiburg, Stefan-Meier Str. 21, 79104 Freiburg, Germany
[c] Institute of Physics, Faculty of Mathematics and Physics, Albert-Ludwig-University of Freiburg, Hermann-Herder-Str. 3, 79104 Freiburg, Germany

ARTICLE INFO

Article history:
Received 8 June 2014
Received in revised form
22 September 2014
Accepted 2 October 2014
Available online 13 October 2014

Keywords:
Cellulose nanocrystals
Ionic liquids
Reaction severity yield optimization

ABSTRACT

We report on near theoretical yield production of cellulose I nanocrystals (CNCs) using a two-step hydrolysis with the mildly acidic ionic liquid (IL) 1-butyl-3-methylimidazolium hydrogen sulfate ([Bmim]HSO_4) in aqueous solution from common cellulosic sources. Two successive Taguchi experimental plans were performed to evaluate the impact of selected reaction parameters (*T*, *t*, H_2O:IL ratio) and their interactions on the CNCs' yield from bleached softwood kraft pulp (SWP), bleached hardwood kraft pulp (HWP) and microcrystalline cellulose (MCC). With these experimental plans, the molar yield for extraction of nanocrystals was optimized to near theoretical levels, reaching 57.7 ± 3.0%, 57.0 ± 2.0%, and 75.6 ± 3.0%, for SWP, HWP and MCC, respectively. The reaction yields corresponded to a relative crystalline region recovery of 84.1 ± 5.3%, 71.7 ± 1.3%, 76.0 ± 2.0% from SWP, HWP and MCC, respectively. The collected nanocrystals exhibited high aspect ratios (36–43), negligible sulfur content (0.02–0.21%) and high solvent dispersibility in comparison to those obtained with the traditional sulfuric acid method. Additionally these near theoretical yields were achieved for mild reaction conditions with the combined severity factor of 2 and 3 for MCC and pulp, respectively. Overall this two-stage IL-mediated preparation of nanocrystals combines the advantages of achieving high product quality, high reaction yields and mild conditions.

1. Introduction

Cellulose nanocrystals (CNCs) have generated increasing attention in the past few years as potential source of novel bionanomaterials (Habibi, 2014; Moon, Martini, Nairn, Simonsen, & Youngblood, 2011; Nishino, Takano, & Nakamae, 1995; Rusli, Shanmuganathan, Rowan, Weder, & Eichhorn, 2011; Sakurada, Nukushina, & Ito, 1962; Sturcova, Davies, & Eichhorn, 2005; Wegner & Jones, 2006). Traditionally, CNCs are isolated from cellulosic resources, such as wood pulp, microcrystalline cellulose and cotton, etc. by concentrated acid hydrolysis (Beck-Candanedo, Roman, & Gray, 2005; Bondeson, Mathew, & Oksman, 2006; Fan & Li, 2012; George, Ramana, Bawa, & Siddaramaiah, 2011). In that purpose, concentrated sulfuric, hydrochloric or phosphoric acid are most commonly used and characterized by rather low reaction yields in the 20–30% range (Bondeson et al., 2006; Camarero Espinosa, Kuhnt, Foster, & Weder, 2013; Lin, Conner, & Hill, 1991; Zhang et al., 2009). To improve production yields for CNCs, new methods have been recently investigated: with cation exchange resin hydrolysis, over 50% CNC yield could be achieved from MCC: this method however requires an additional step for resin removal (Tang, Huang, Ou, Chen, & Chen, 2011); a one-step method for CNCs preparation and surface carboxylation has also been reported with ammonium persulfate, whereby 65% and 81% of CNCs were obtained from MCC, cotton, respectively (Hu et al., 2014; Leung et al., 2011). Ball milling of a mixture of maleic anhydrate, sulfuric acid and wood pulp before hydrolysis under ultrasonication (7 h, 75 °C) has resulted in ca. 61% yields of cellulose I nanocrystals (Tang, Huang, Yang, et al., 2013). A yield of ca. 40% of CNCs has been achieved from MCC with ultrasonic-assisted sulfuric acid hydrolysis (Tang, Yang, Zhang, & Zhang, 2014); it increased to ca. 55% with microwave-assisted acid hydrolysis from reed pulp (Zhao, Liu, & Zhang, 2012); 64.1% of

* Corresponding author at: Chair of Forest Biomaterials, Faculty of Environment and Natural Resources, Albert-Ludwig-University of Freiburg, Werthmannstr. 6, 79085 Freiburg, Germany. Tel.: +49 76120397617.
E-mail address: marie-pierre.laborie@biomat.uni-freiburg.de (M.-P. Laborie).

http://dx.doi.org/10.1016/j.carbpol.2014.10.001
0144-8617/

CNCs could be collected from beaten cotton using the sulfuric acid hydrolysis (Fan & Li, 2012); 85% of CNCs has been obtained from cotton with a mixture of sulfuric acid and acetic acid hydrolysis followed by sonication for 5 h (Tang, Huang, Lu, 2013). Using heteropoly acid (phosphotungstic acid, $H_3PW_{12}O_{40}$), CNCs with high surface stability have been produced in 60% yield (Liu et al., 2014). Hydrochloric acid (21.2 w%) under severe hydrothermal treatment leads to near theoretical yields of ca. 90% from MCC (Yu et al., 2013). These processes however consume significant amounts of corrosive acids and might be further improved from the environmental standpoint (Li & Zhao, 2007).

Following the work of Man et al. (2011), it was recently demonstrated that CNCs can be produced from MCC in relatively high yields of 48 ± 2 w% using a mildly acidic ionic liquid (IL) viz. 1-butyl-3-methylimidazolium hydrogen sulfate ([Bmim]HSO_4 (Mao, Osorio-Madrazo, & Laborie, 2013). While this yield remains low compared to theoretical yields based on MCC crystallinity, it has the advantage of using milder conditions; in fact the [H+]/[AGU] ratio is decreased by an order of magnitude with this route. A potential optimization route was suggested there by decoupling the process into (1) swelling stage for opening cellulose structure and (2) a water-triggered hydrolysis of the swollen cellulose. Such a two-step extraction approach for CNCs has been successfully taken by Lazko et al. (2014) using [Bmim]Cl.

This study reports on the use of such decoupled route in combination with Taguchi factorial experimental designs to achieve near theoretical yields for CNCs production from MCC and wood pulps with [Bmim]HSO_4. In particular, Taguchi experimental plans are applied to evaluate the impact of temperature (T), time (t), (H_2O:IL) mass ratio and their interactions: $T \times t$, $T \times H_2O$:IL, $t \times H_2O$:IL, $T \times t \times H_2O$:IL on yield as well as the characteristics of the nanocrystals. In doing so, near theoretical yields of high quality cellulose I nanocrystals are achieved from hardwood pulp, softwood pulp and MCC under low reaction severity.

2. Experimental

2.1. Optimization of cellulose nanocrystals (CNCs) production with [Bmim]HSO_4 materials

Bleached softwood (Scots Pine, *Pinus* sylvestris) kraft pulp (SWP) and bleached hardwood (Birch, *Betula*) kraft pulp (HWP) were provided by Stora Enso (Imatra Mills, Finland). Microcrystalline cellulose (Avicel, PH-101) (MCC) and 1-butyl-3-methylimidazolium hydrogen sulfate ([Bmim]HSO_4) were purchased from Sigma Aldrich. The crystallinity index (CrI) of SWP, HWP and MCC were estimated at 54%, 61% and 82%, respectively, based on X-ray diffraction measurements. The materials were oven-dried prior to use.

2.1.1. Reaction procedure and Taguchi experimental plans

For the production of nanocrystals, a two-step route was employed. Firstly, the cellulosic material (0.81 g) was swollen in pure IL by mixing into a 250 ml triple neck round bottom flask at room temperature for 24 h. Secondly, deionized water (DI–I) was added in controlled amounts in order to initiate the acid-catalyzed hydrolysis from the hydrogen sulfate. In a typical run, the reaction was quenched with liquid nitrogen and the suspension repeatedly centrifuged at 12,000 rpm for 10 min (F15 6X100Y Multifuge, Thermo Scientific, MA, USA) and washed to collect the turbid supernatant, containing the crystals. The turbid supernatant was then dialyzed against DI water until pH≈6–7 and reaction yield was gravimetrically obtained after freeze-drying (ALPHA 1 2 LD plus freeze dryer, Martin Christ, Osterode am Harz, Germany). To optimize the reaction yield, Taguchi experimental plans were designed based on 3 factors viz. (H_2O:IL) mass ratio, reaction temperature (T), reaction time (t) and their respective interactions viz. $T \times t$, $T \times H_2O$:IL, $t \times H_2O$:IL, $T \times t \times H_2O$:IL at two levels according to $L2^7$ experimental tables. Taguchi factorial plans allow deciphering factor impacts on the response (yield); and optimizing a process in a minimum number of experiments. Two successive $L2^7$ experimental tables were necessary for each raw material in order to achieve near-theoretical yields (Tables 1 and 2). For all reactions, the liquid-to-solid mass ratio was maintained at 84:1 for the wood pulps and 10:1 for MCC.

2.2. Severity factor and crystalline recovery of the reaction

The combined reaction severity factor (CSF) was calculated (Chum et al., 1988; Overend, Chornet, & Gascoigne, 1987):

$$\mathrm{CSF} = \mathrm{Ro} - \mathrm{pH} = \log\left[t \times e^{\frac{(T-T_{\mathrm{ref}})}{10.75}}\right] - \mathrm{pH}$$

where, Ro is the severity factor, t is the reaction time (min), T is the reaction temperature (°C) and T_{ref} is a reference temperature most often set at 100 °C, pH is the initial pH value of the reaction.

Relative crystalline region recovery (CR) and relative amorphous region removal (AR) were calculated as an additional way to assess the reaction efficiency. This calculation was based on the assumption that apparent crystallinity linearly relates to crystallinity index and that the native crystal shape is unaffected by processing:

$$\mathrm{CR}(\%) = \frac{M_{\mathrm{CNCs}} \times \mathrm{CrI}_{\mathrm{CNCs}}}{M_o \times \mathrm{CrI}_o} \times 100 = Y_w \frac{\mathrm{CrI}_{\mathrm{CNCs}}}{\mathrm{CrI}_o} \times 100$$

$$\mathrm{AR}\ (\%) = \frac{M_o \times (1 - \mathrm{CrI}_o) - M_{\mathrm{CNCs}} \times (1 - \mathrm{CrI}_{\mathrm{CNCs}})}{M_o \times (1 - \mathrm{CrI}_o)} \times 100$$

$$= \left(1 - Y_w \frac{1 - \mathrm{CrI}_{\mathrm{CNCs}}}{1 - \mathrm{CrI}_o}\right) \times 100$$

where M_{CNCs}, $\mathrm{CrI}_{\mathrm{CNCs}}$ and M_o, CrI_o are the mass and the crystallinity index of CNCs and raw material, respectively; Y_w is the gravimetric yield of CNCs.

2.3. Morphological characterization of cellulose nanocrystals

Once the reaction conditions had been optimized for the highest yield with each of the three cellulosic materials, the obtained crystals were characterized for morphology (AFM, XRD), crystallite dimensions, surface chemistry and dispersibility in various solvents.

2.3.1. Atomic force microscopy (AFM)

A droplet of the dilute CNCs suspension was allowed to dry overnight on freshly cleaved mica before observation in tapping mode with an AFM (Nanoscope III) equipped with a tube scanner from Digital Instruments (Veeco Santa Barbara, CA, USA) using silicon tips (PPP-NCH, Nanoandmore, Wetzlar, Germany) with resonance frequency and spring constant of 360 kHz and 50 N/m, respectively. The height images were analyzed with a Nanoscope Analysis 1.4 software and the dimensions of the CNCs were determined. To circumvent tip-broadening effects, the width was obtained from a height scan across crystals. Number-average length and width were computed from over 100 measurements.

2.3.2. Fourier transform infrared spectroscopy (FTIR)

The raw materials and derived nanocrystals were characterized in transmission mode on a FT-IR Spectrometer 65 (Perkin Elmer, Massachusetts, USA). KBr pellets comprising 10 mg of material with a mass ratio of 1:100 to KBr and 64 cumulative scans were acquired with a resolution of 4 cm^{-1} in the 4000–650 cm^{-1} range.

Table 1
First Taguchi L2[7] table indicating the experimental levels (1, 2) selected for each factor and interaction and the main response for the bleached softwood kraft pulp (SWP), hardwood kraft pulp (HWP), and microcrystalline cellulose (MCC).

Exp.	Factor and interaction level							Mass yield (w%)		
	T (°C)	t (h)	$T \times t$	H_2O:IL (w/w)	$T \times H_2O$:IL	$t \times H_2O$:IL	$T \times t \times H_2O$:IL	SWP	HWP	MCC
1	65	6	1	0:1	1	1	1	0	0	19
2	65	6	1	0.5:0.5	2	2	2	0	0	41
3	65	24	2	0:1	1	2	2	0	0	27
4	65	24	2	0.5:0.5	2	1	1	7	6	20
5	120	6	2	0:1	2	1	2	9	9	56
6	120	6	2	0.5:0.5	1	2	1	21	29	37
7	120	24	1	0:1	2	2	1	15	16	21
8	120	24	1	0.5:0.5	1	1	2	41	52	66

2.3.3. Wide angle X-ray diffraction (WAXD)

WAXD measurements were carried out on the raw materials and the corresponding obtained CNC powders. To avoid orientation, the samples were grinded (disk-milling with wood pulp and hand-milling with CNCs) and then filled in a brass sample holder without applying any pressure. X-ray scattering curves were recorded in reflexion mode in the 2θ-range of 2–70° with a resolution higher than 0.3° using the D500 X-ray powder diffractometer (Siemens, Germany) with CuKα radiation ($\lambda = 0.1542$ nm).

Cellulose crystallinity index (CrI) was calculated from the crystalline (I_{200}) and amorphous (I_{am}) signal intensities at $2\theta = 22.4°$ and at $2\theta = 18°$, respectively (Segal, Creely, Martin, & Conrad, 1959).

$$\mathrm{CrI} = \frac{I_{200} - I_{am}}{I_{200}} \times 100$$

Coherence lengths of the crystallites were determined for two directions, i.e., thicknesses τ were derived from the [2 0 0] reflection at $2\theta = 22.4°$ and lengths B from the [0 0 4] reflection at $2\theta = 34.5°$ applying the Scherrer equation (Guinier, 1963; Strobl, 2007).

$$\tau = \frac{2\pi}{\Delta q_{200}} \quad \text{and} \quad B = \frac{2\pi}{\Delta q_{004}}$$

with scattering vector $q = 4\pi/\lambda \sin\theta$. The integral line width Δq_{200} was calculated from the peak width of the Gaussian representing the [2 0 0] Bragg reflection, however the integral line width Δq_{004} of the [0 0 4] reflection was obtained directly by integration.

2.3.4. Surface properties of nanocrystals

The sulfur content of the nanocrystals was estimated from elemental analysis on an Elemental analyzer Vario EL (Elementar Analysensysteme, Hanau, Germany). This allowed estimating the sulfate ester degree of substitution (DS), the molar mass of the partially substituted anhydroglucose (AGU), and therefore computing molar yields:

$$\mathrm{DS} = n_s \times 6/n_c = (S\%/32) \times 6/(C\%/12) = 9S\%/4C\%$$

$S\%$, $C\%$: mass percentage of S and C from elemental analysis; n_S, n_C: moles of S and C.

$$n_{\mathrm{CNCs}} = M_{\mathrm{CNCs}}/162 + 80 \times \mathrm{DS}$$

n_{CNCs}: moles of CNCs; M_{CNCs}: mass of the obtained CNCs; 162 (g/mol): molecular weight of AGU; 80 (g/mol): molecular weight of sulfate group; DS: degree of substitution of CNCs.

Additionally, dispersibility of CNC particles was tested by mixing 3 mg freeze-dried CNCs per mL of solvent with non-polar solvents (toluene, chloroform), polar aprotic solvents (tetrahydrofuran (THF), dimethyl sulfoxide (DMSO)) and polar protic solvents (acetic acid and water). Dispersibility and stability of the dispersion was visually assessed after 5 h, 5 days and one month after following 24 h mixing.

3. Results and discussion

3.1. Reaction factor and yield optimized from Taguchi plans

It is clear that reaction factors and their interactions can play a significant role in the reaction efficiency. Knowledge of significant factors and interactions is of fundamental interest and of practical importance to optimize the reaction, as demonstrated in previous studies using the concentrated acid method (Bondeson et al., 2006; Dong & Roman, 2012). However, a comprehensive study of the impact of reaction factors and their interaction in the [Bmim] HSO_4 route is lacking. A comprehensive understanding of the impact of each factor on a reaction is best gathered from factorial experimental designs, such as Taguchi plans. Table 1 illustrates the 8 experimental conditions of the L2[7] experimental table first used on the three cellulosic materials. Note that each factor and interaction is either set at level 1 (65 °C for T, 6 h for t, 0:1 for H_2O:IL ratio) or level 2 (120 °C for T, 24 h for t, 0.5:0.5 for H_2O:IL ratio). Additionally, the measured gravimetric yield is reported. It reaches its highest values of 41 w%, 52 w% and 66 w% for SWP, HWP and MCC respectively for the highest reaction temperature and time (level 2,

Table 2
Second Taguchi L2[7] table indicating the experimental levels (1, 2) selected for each factor and interaction and the main response for the bleached softwood kraft pulp (SWP), hardwood kraft pulp (HWP), and microcrystalline cellulose (MCC).

Exp.	Factor and interaction level							Mass yield (w%)		
	T (°C)	t (h)	$T \times t$	H_2O:IL (w/w)	$T \times H_2O$:IL	$t \times H_2O$:IL	$T \times t \times H_2O$:IL	SWP	HWP	MCC
1	100	12(3)[a]	1	0.25:0.75	1	1	1	30	37	23
2	100	12(3)	1	0.75:0.25	2	2	2	3	0	24
3	100	36(12)	2	0.25:0.75	1	2	2	55	37	78
4	100	36(12)	2	0.75:0.25	2	1	1	11	10	45
5	130	12(3)	2	0.25:0.75	2	1	2	60	56	62
6	130	12(3)	2	0.75:0.25	1	2	1	26	22	17
7	130	36(12)	1	0.25:0.75	2	2	1	35	45	43
8	130	36(12)	1	0.75:0.25	1	1	2	10	12	54

[a] Reaction time of MCC shows in the ().

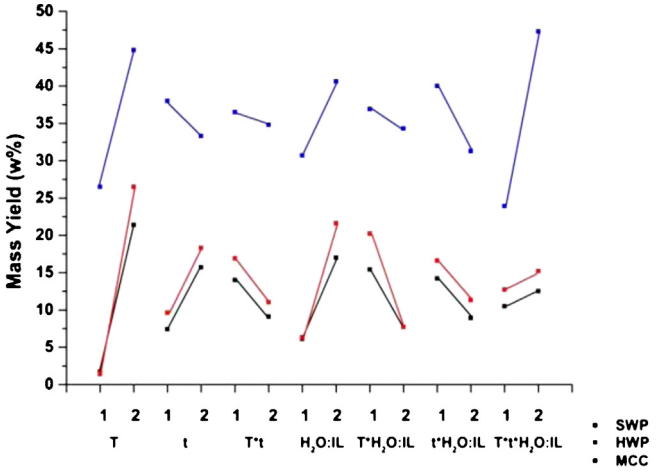

Fig. 1. The response of process factors (T, t, H_2O:IL), and their interactions for nanocrystal production from softwood kraft pulp (SWP), hardwood kraft pulp (HWP), and microcrystalline cellulose (MCC) based on the first Taguchi plan.

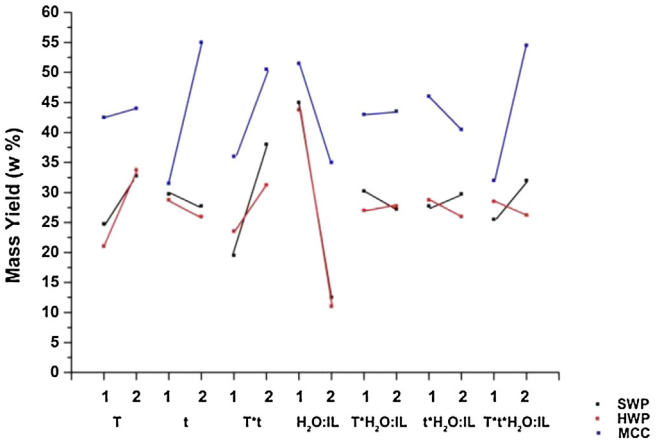

Fig. 2. The response for process factors (T, t, H_2O:IL), and their interactions for nanocrystal production from softwood kraft pulp (SWP), hardwood kraft pulp (HWP), and microcrystalline cellulose (MCC) based on the second Taguchi plan.

120 °C, 24 h and 0.5:0.5). These yields are well above the reported yield with traditional sulfuric acid treatments (20–30% for pulp) (Beck-Candanedo et al., 2005; Hamad & Hu, 2010; Wang, Ding, & Cheng, 2007); or with a similar ionic liquid system performed in one stage (Mao et al., 2013). Reaction yield can thus be largely improved when fewer protons are mobilized on a fully swollen cellulose substrate.

The importance of each factor and level towards the yield is best seen on the figure of responses (Fig. 1). The largest changes in response between the two levels are seen for the temperature factor followed by the H_2O:IL ratio, while other factors display less impact on the yield (difference <10%). This is true regardless of the cellulose source, with the particularity that there is a very significant interaction between all 3 factors for MCC. Higher temperature (120 °C) and higher water content (H_2O:IL ratio of 0.5:0.5) appear favorable to the yield within the levels assessed in this first Taguchi plan.

This information was used to design a subsequent Taguchi plan for further optimization (Table 2). Accordingly yields in this second Taguchi plan further increase, reaching 58 w%, 57 w% and 76 w% from SWP, HWP, and MCC, respectively. Again, for pulp, temperature and (H_2O:IL) mass ratio are the most important factors in the

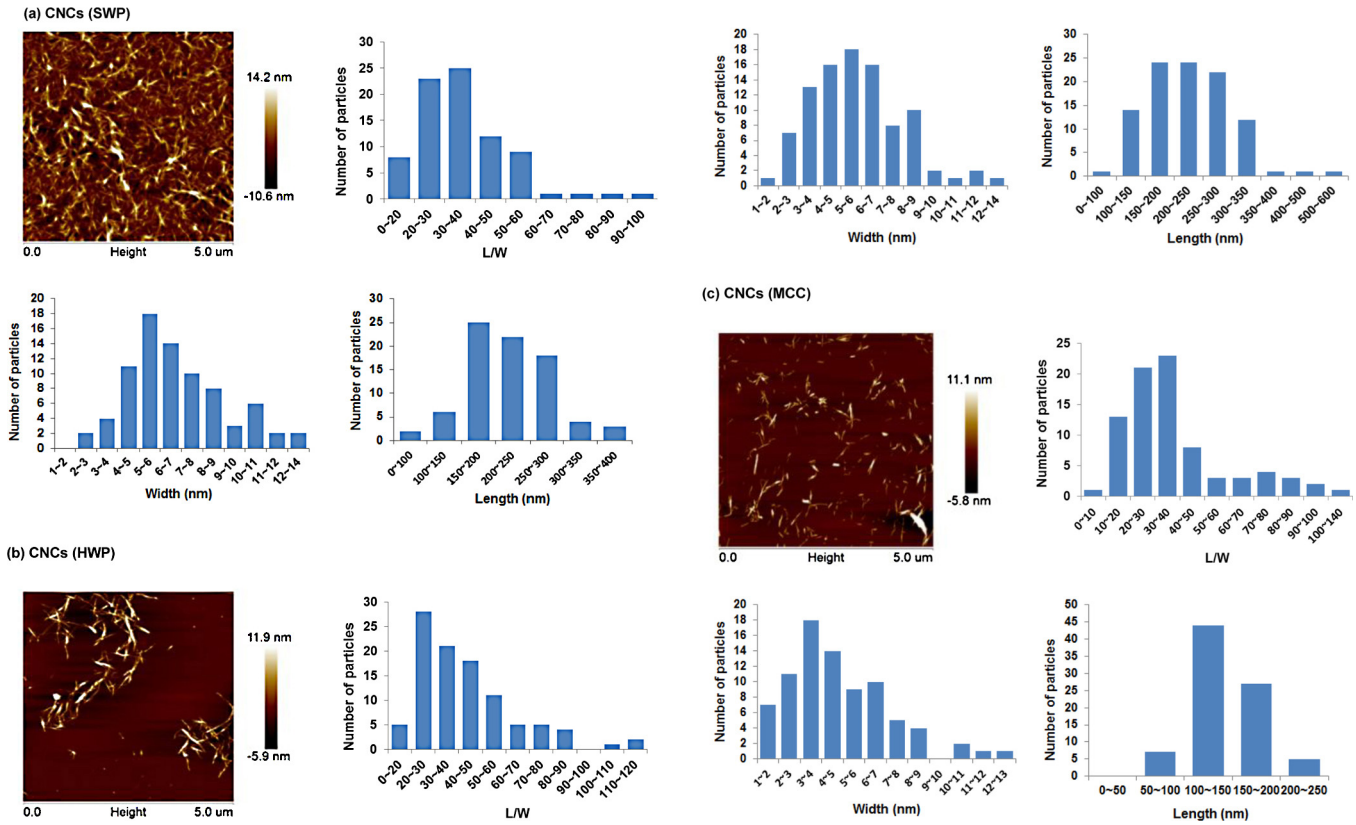

Fig. 3. AFM height images, aspect ratio (L/W), width and length distributions evaluated from AFM images of CNCs obtained after treating with [Bmim]HSO_4 from (a) SWP, (b) HWP and (c) MCC.

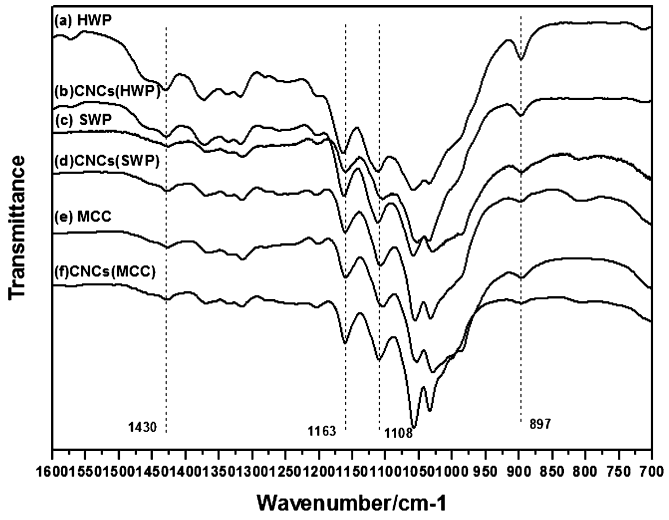

Fig. 4. FTIR spectra of starting materials (a) HWP, (c) SWP, (e) MCC and nanocrystals produced thereof with the two-stage [Bmim]HSO_4 (b) CNCs (HWP), (d) CNCs (SWP) and (f) CNCs (MCC).

range tested; higher temperature (130 °C) and lower (H_2O:IL) content are favorable (Fig. 2). Starting from MCC, reaction time (12 h) and interaction among all factors remain the most significant factors. The highest mass yields obtained from SWP, HWP and MCC are well above those previously reported with the traditional sulfuric acid method (Beck-Candanedo et al., 2005; Bondeson et al., 2006; Elazzouzi-Hafraoui et al., 2008).

With two successive $L2^7$ orthogonal arrays of experiments, the production was optimized to approach theoretical yields for each of the three cellulosic sources. With the two-stage-IL approach hereby devised, the optimum conditions for gravimetric yield are reaction time of 12 h, mass ratio of H_2O:IL of 2.5:7.5, reaction temperature of 130 °C for wood pulp and 100 °C for MCC, respectively. When trying to further optimize the important factors, the yield started to decrease, suggesting that the optimum had already been reached with this particular chemical route and this two-stage approach.

3.2. Crystal quality with the two-stage [Bmim]HSO_4 route from SWP, HWP and MCC

AFM height images confirm that rod-like nanoparticles are obtained from all three cellulose sources using this two-step IL route (Fig. 3a–c). Width averaged 7 ± 2, 6 ± 2, 5 ± 2 nm and length was around 230 nm and 145 ± 36 nm when starting from SWP, HWP, MCC respectively (Table 3). These are similar in size to those produced by concentrated acid (Beck-Candanedo et al., 2005; Wang et al., 2007). Also a slightly higher aspect ratio (L/W) (35–45 on average) with a broader distribution is observed for the IL-produced CNCs compared to those produced with the sulfuric acid method (Bai, Holbery, & Li, 2009; Eichhorn, 2011; Mathew & Dufresne, 2002).

Further chemical and morphological information is obtained by comparing the FTIR spectra of SWP, HWP, MCC and the respective CNCs (Fig. 4). For the obtained crystals, characteristic peaks at 1429 cm^{-1} (CH_2 scissoring), 1161–1163 cm^{-1} (C—O stretching or O—H bending) and 897 cm^{-1} for C_1 vibrational mode, respectively suggest that the native cellulose I allomorph is retained (Nelson & O'Connor, 1964). The pronounced band at 1111 cm^{-1} is strongly indicative of cellulose I microstructure while the presence of cellulose II is not evidenced on these spectra (Magalhaes, Cao, & Lucia, 2009). Higher crystallinity in the nanocrystals compared to the raw materials is furthermore evident from the intensity increase at 1058 cm^{-1} and 1034 cm^{-1} (C—O—C stretching) (Oh et al., 2005).

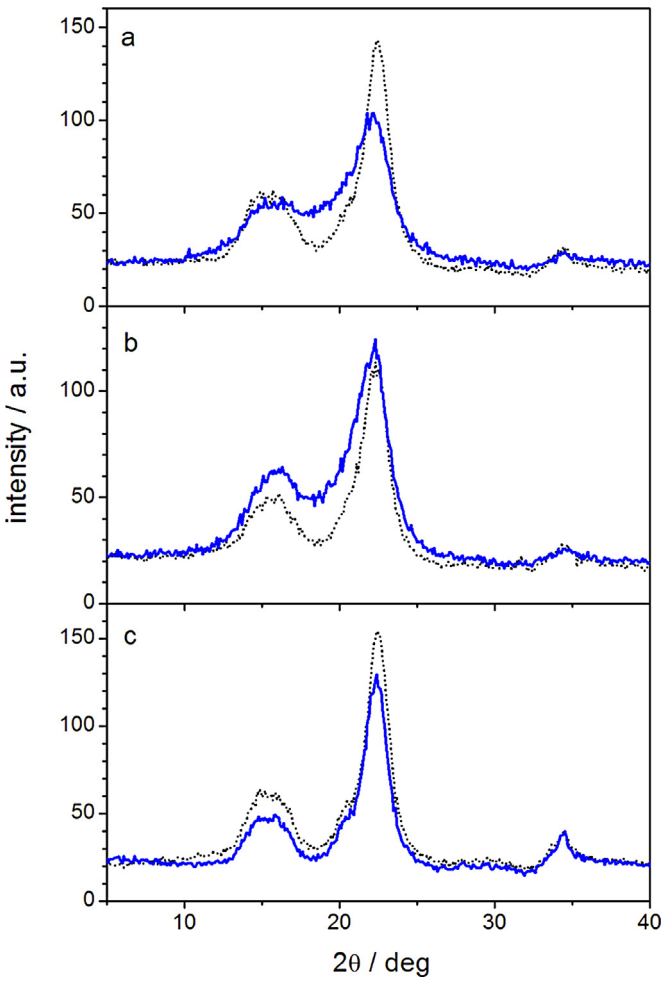

Fig. 5. X-ray diffraction patterns of the starting materials (solid lines) (a) SWP, (b) HWP and (c) MCC and the obtained CNCs in the highest mass yield from each material (dotted lines).

Note also the absence of S=O stretching band at 1068–1076 cm^{-1}, which suggests a low surface modification of cellulose with sulfate esters during preparation with [Bmim]HSO_4 (Zhang, Brendler, & Fischer, 2010).

WAXD is further used to shed light on the crystalline microstructure of the produced CNCs in comparison to the raw materials (Fig. 5). All three CNCs exhibit the typical cellulose I characteristic peaks at 2θ equal to 14.8°, 16.3°, 20.4°, 22.4° and 34.5° corresponding to the crystallographic planes [−1 1 0], [1 1 0], [1 0 2], [2 0 0] and [0 0 4], respectively (Nishiyama, Langan, & Chanzy, 2002; Nishiyama, Sugiyama, Chanzy, & Langan, 2003). The absence of cellulose II peak around 12° of 2θ indicates that cellulose regeneration into cellulose II does not occur in this two-stage IL route. Compared with the starting pulp for softwood and hardwood, Segal crystallinity (CrI) increases from 54% to 78 ± 1 and from 61% to 77 ± 1, respectively (Table 3). Nanocrystals for MCC have the same CrI as the raw material (82%) (Table 3). These values are in agreement with the literature: the crystallinity index of CNCs has been reported between 78% and 82% for pulps, 70% and 90% for MCC, depending on the reaction conditions (Beck-Candanedo et al., 2005; Hermans, 1950; Herrera, Mathew, & Oksman, 2012; Landry, Alemdar, & Blancher, 2010; Li, Yue, & Liu, 2012; Moon et al., 2011).

The coherence lengths of the crystallites in the width and length directions are determined from the reflections [2 0 0] and [0 0 4] in both raw materials and CNCs (Table 3). The thickness of the crystallites is 4.2 nm in both wood pulps, and 4.7 nm in MCC,

Table 3
Characteristics of cellulose nanocrystals obtained in the two-step [Bmim]HSO_4-mediated hydrolysis from SWP, HWP and MCC.

Raw material		SWP	HWP	MCC
Optimal condition	T (°C)	130	130	100
	t (h)	12	12	12
	H_2O:IL (w/w)	2.5:7.5	2.5:7.5	2.5:7.5
Reaction efficiency	Y_w (%)	57.8 ± 2.9	57.1 ± 1.9	76.0 ± 3.0
	Y_{mol} (%)	57.7 ± 3.0	57.0 ± 2.0	75.6 ± 3.0
	CR (%)	84.1 ± 5.3	71.7 ± 1.3	76.0 ± 2.0
	AR (%)	72.7 ± 0.4	65.9 ± 2.9	24.0 ± 7.7
Surface chemistry	S (%)	0.06 ± 0.05	0.02 ± 0.03	0.21 ± 0.03
	DS (%)	0.3 ± 0.3	0.2 ± 0.1	1.1 ± 0.2
CNCs morphology	L (nm)	219 ± 68	227 ± 74	143 ± 36
	W (nm)	7 ± 2	6 ± 2	5 ± 2
	L/W	36 ± 16	43 ± 21	38 ± 21
	CrI index (%)	78 ± 1	77 ± 1	82 ± 1

Crystallites morphology	τ (nm); B (nm)				
		Raw material	4.2; 5	4.2; 5	4.7; 7
		CNCs	4.6 ± 0.2; 6 ± 1	4.4 ± 0.2; 6 ± 1	4.9 ± 0.2; 6 ± 1

while the length of SWP, HWP and MCC is 5, 5 and 7 nm, respectively. Similar thickness has been previously reported for wood pulp (4.3–5.1 nm) and for MCC (4.6–5.7 nm) (Fink, Hofmann, & Philipp, 1995; Garvey, Parker, & Simon, 2005; Leppänen et al., 2009; Majdanac, Poleti, & Teodorovic, 1991; Revol, Dietrich, & Goring, 1987; Thygesen, Oddershede, Lilholt, Thomsen, & Ståhl, 2005). The crystallite length for both wood pulps and MCC has been reported to range from 6.4 nm to 30.4 nm (Andersson, Serimaa, Paakkari, Saranpää, & Pesonen, 2003; Leppänen et al., 2009; Thygesen et al., 2005). The thickness of the crystallites in CNCs for all materials is also comparable with the reported crystallite thickness of 4.3–5.0 nm (Elazzouzi-Hafraoui et al., 2008; Jiang, Esker, & Roman, 2010), and is slightly higher than in the starting material, suggesting size-fractionnation during the IL treatment. Note that the crystallite coherence length in width and length directions as measured by WAXD are slighly higher than dimensions measured by AFM. This is expected and suggests that the native monocrystals are covered by a layer of less organized material.

3.3. Sulfur content and dispersibility

During HSO_4^--mediated hydrolysis of cellulose, sulfate ester groups functionalize the nanocrystals. Elemental analysis (Table 3) shows a small amount of sulfur (0.21 ± 0.03% from MCC, 0.06 ± 0.05% from SWP and 0.02 ± 0.03% from HWP) compared to that reported with the concentrated sulfuric acid route (MCC: S: 0.53–0.75%, softwood pulp: S: 0.92%) (Abitbol, Kloser, & Gray, 2013; Dong, Revol, & Gray, 1998; Hamad & Hu, 2010). Based on elemental sulfur content, a DS of 0.011 is calculated from MCC with the present IL route, which compares favorably with the DS reported with concentrated sulfuric acid in the 0.04–0.07 (Hamad & Hu, 2010). Similarly, low degree of substitution is observed for CNCs obtained from the wood pulps. The observation that lower sulfation extent occurs in CNC produced with ionic liquids is consistent with previous studies and has been shown to enhance thermal stability (Lazko et al., 2014; Mao et al., 2013).

Knowing this DS, the gravimetric yield of the reaction can be converted into a molar yield, which in this case involves a small reduction of 0.1–0.4%.

CNCs obtained with the ionic liquid-based method therefore bear less surface charges than those obtained with the concentrated sulfuric acid. The impact of surface charge and chemistry on solvent dispersibility is critical for the application of nanocrystals in composites. In Fig. 6, the dispersion of CNCs in six different solvents, namely, two non-polar solvents: toluene, chloroform; two polar aprotic solvents: THF, DMSO; two polar protic solvents: acetic acid, H_2O, is shown. CNCs suspensions in water remain homogenous after one month, which indicates that the amount of surface charges is sufficient for the repulsion to stabilize them. With low dielectric solvents, dispersibility becomes weaker, which leads to phase separation; with protic solvent acetic acid, the mixture is unstable after 5 h due to the lower dielectric constant. CNCs are not dispersed in toluene at all.

3.4. Discussion: on the use of a two-stage IL approach for maximum cellulose crystal recovery

The CNCs molar yield was optimized to 57.7 ± 3.0%, 57.0 ± 2.0% and 75.6 ± 3.0% from SWP, HWP and MCC with relatively high cellulose I crystallinity index of 78 ± 1%, 77 ± 1% and 82 ± 1%, respectively. Such yield for nanocrystal production in a mild one-pot reaction is higher than that obtained with the traditional approach. For example, with one-pot concentrated sulfuric acid hydrolysis, yields are reported in the 20–30% range and our previous study with the one-step IL-mediated reaction yielded 48 ± 2% from MCC, viz. 2/3 of the current yield. This illustrates the power of the two-step procedure, namely achieving maximal swelling to enhance the accessibility to the amorphous domains for further hydrolysis with water-triggered H^+ released from the IL. Also note that the molar ratio of acid to anhydroglucose ([H+]/[AGU]) is low, viz. 0.29 mol/mol and 2.43 mol/mol for the two-step IL-based reaction. This ratio is 10–100 times lower than that used in the concentrated acid approach. In fact, the combined severity factor (CSF) helps evaluate the harshness of the reaction conditions as well, in light of the yield. In Fig. 7, yield generally increases with severity factor up to an optimum. This optimum yield is found at a CSF of around 3 for both wood pulp and about 2 for MCC. This confirms that the successive Taguchi plans have allowed a rapid identification of optimum conditions. Additionally, this illustrates that less stringent conditions are required to efficiently produce CNCs from MCC compared to wood pulp. Severity factor for the concentrated acid method is also computed and compared to the IL-mediated method. The highest yields of 93% and 81% from MCC and from wood pulp have been achieved with a CSF of around 3.33 (Yu et al., 2013), which is higher than with the IL-mediated method (CSF of 2.83 and 2.13) and the strong acid methods (0.5–2).

Concentrated acid can not only hydrolyze the amorphous fraction of cellulose, it can also dissolve it; in comparison, [Bmim]HSO_4 is a poor solvent for cellulose, but can be used as a good swelling agent, while its moderate to weak acidic character (anion HSO_4^-) can initiate cellulose hydrolysis. It can explain the improved efficiency of the few protons available in the system, while delivering more homogeneous nanocrystals (Mao et al., 2013). In order to

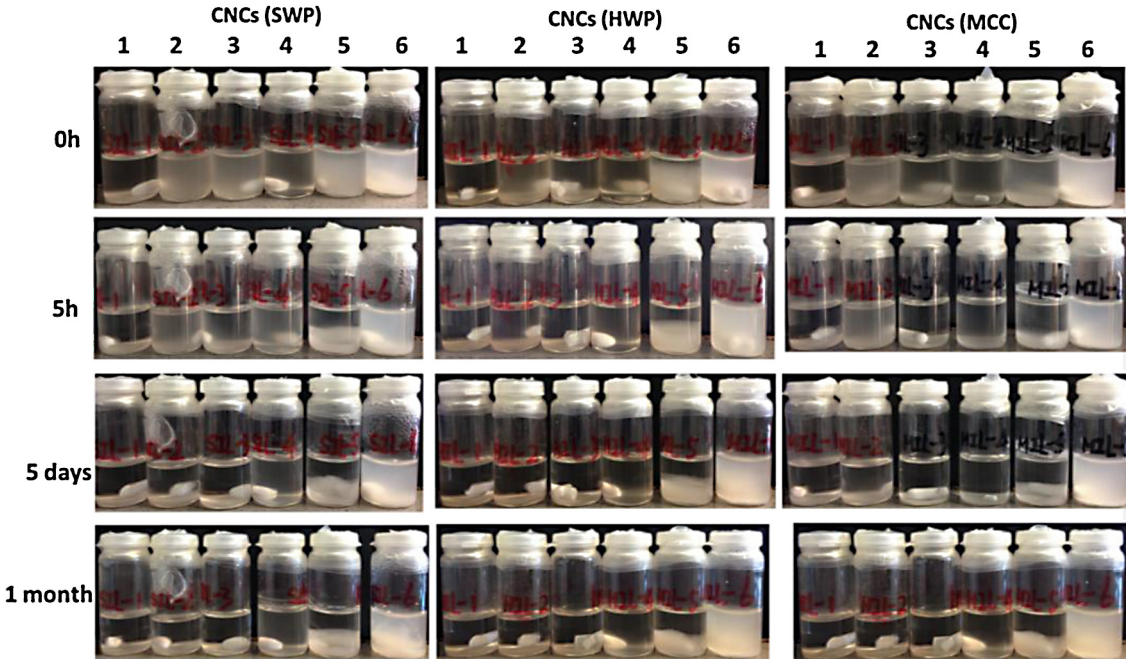

Fig. 6. Photos of suspensions of CNCs from SWP, HWP and MCC in six different solvents: (1) toluene; (2) chloroform; (3) THF; (4) DMSO; (5) acetic acid; (6) H_2O. The photos were taken the moment after magnetic stirring overnight (0 h), 5 h, 5 days and one month after preparation.

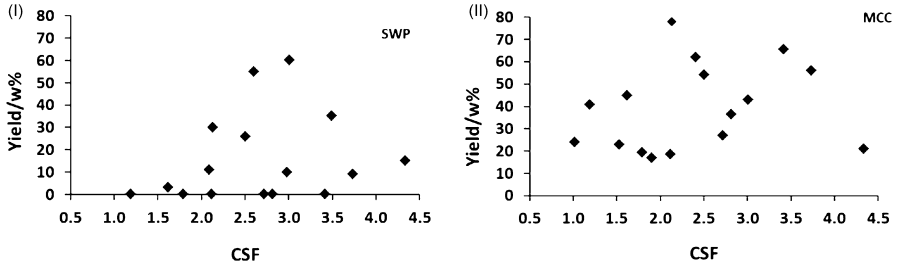

Fig. 7. Mass yield of CNCs as a function of combined severity factor (CSF) for (I) bleached softwood kraft pulp (SWP), (II) MCC. Similar behavior was observed with HWP and is not shown.

further characterize the reaction efficiency with all starting materials, the "relative crystalline region recovery (CR)" and "relative amorphous region removal (AR)" were computed. Ideally the mass of the produced CNCs with 100% of crystallinity should equal the mass of crystalline region in the raw material; however, one distinct scenario is observed for each cellulose source: crystals from MCC have similar crystallinity index (ca. 82%) than MCC itself. With the reaction yield approaching 78 w%, it can be deduced that 76% of the crystalline fraction is recovered and 24% of the amorphous fraction is removed. The removed fraction of crystalline cellulose (24%) probably comes from the reaction and operation loss during the process. Cellulose degradation or dissolution might happen as well. In comparison, for hardwood and softwood pulps the opposite trend is observed: around 73% and 66% of amorphous fractions is removed while the crystalline loss is kept minimal at around 16% and 28%, respectively. Note that compared to the CR with one-step IL-mediated method (45.1%) (Mao et al., 2013), almost twice of the crystalline fractions can be recovered when using the two-step method. CR and AR are possibly related to the crystallinity index of the raw material (Fig. 8). The more amorphous fraction the starting cellulosic source contains, the more efficiently the amorphous fraction is removed during the process. Such behavior can be explained based on diffusion rates and higher accessibility for an heterogeneous hydrolysis in more amorphous substrate (Abasaeed, Lee, & Watson, 1991). Similarly, the retained amorphous fraction from all three raw materials is the same as expected from the crystals

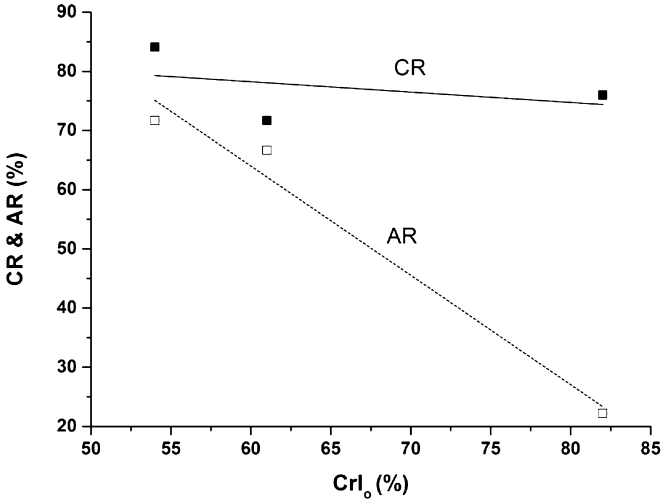

Fig. 8. Relative crystalline recovery (CR) and amorphous removal (AR) as a function of crystallinity index (CrI_o) of the raw material.

morphology, whereby a rigid amorphous phase is coating the cellulose crystallites and cannot be removed. This is expected since the proportion of amorphous to crystalline domains is similar and is dictated by the molecular parameters (Peterlin & Zachmann, 1971).

The high yield obtained further demonstrates the power of factorial design of experiments to optimize a process in a minimum amount of experiments. However with the concept of crystalline recovery one also clearly sees that improvements are further possible, since ca. 84%, 72% and 76% of native crystals are recovered from SWP, HWP and MCC respectively. Overall the yield is improved from 60% to 160% compared to previous reports, while maintaining the reactant recyclability as previously demonstrated with this route (Mao et al., 2013). Further analysis is however needed to assess to economical and environmental viability of the IL-mediated production method and is currently ongoing in our laboratory.

4. Conclusion

Taguchi experimental plans were used to optimize the production yield of cellulose I nanocrystals with a two-stage mildly acidic IL-mediated hydrolysis approach and to evaluate the impact of the preparation factors and their interactions on the process yield. Near theoretical molar yields of $57.7 \pm 3.0\%$, $57.0 \pm 2.0\%$, and $75.6 \pm 3.0\%$ were obtained from SWP, HWP and MCC, respectively. The cellulose I nanocrystals exhibit favorable properties: high aspect ratios (35–45), low sulfur content (0.02–0.2%) and good stability in a variety of solvents. Less severe conditions were required to efficiently produce crystals starting from MCC than from wood pulp. High relative crystalline region recoveries of $84.1 \pm 5.3\%$, $71.7 \pm 1.3\%$, $76.0 \pm 2.0\%$ were achieved from SWP, HWP and MCC, respectively, with the same amount of amorphous fraction retained. This confirmed that native cellulose crystallites, with their amorphous layer coating, were collected from all raw materials. The low severity factor of the optimized reaction, the high reaction yield and crystal quality together with the ability to recycle the ionic liquid as previously demonstrated place this approach as a method of choice for the collection of native cellulose I nanocrystals from a variety of cellulosic sources. Slight yield improvements still appear possible.

Acknowledgements

This research was partially supported from the European Union, through the Baden-Württemberg Ministry Program: Cluster initiative Forst und Holz. Jia Mao acknowledges a scholarship from the Elisabeth und Barbara Grammel foundation at the University of Freiburg. Dr. Werner Lux, from Sappi Ehingen provided bleached wood pulps; Elke Stibal provided technical assistance. Dr. Alfred French (USDA-ARS) is also greatly acknowledged for discussions and support in crystallographic analysis.

References

Abasaeed, A. E., Lee, Y. Y., & Watson, J. R. (1991). Effect of transient heat transfer and particle size on acid hydrolysis of hardwood cellulose. *Bioresource Technology*, *35*(1), 15–21.

Abitbol, T., Kloser, E., & Gray, D. G. (2013). Estimation of the surface sulfur content of cellulose nanocrystals prepared by sulfuric acid hydrolysis. *Cellulose*, *20*(2), 785–794.

Andersson, S., Serimaa, R., Paakkari, T., Saranpää, P., & Pesonen, E. (2003). Crystallinity of wood and the size of cellulose crystallites in Norway spruce (*Picea abies*). *Journal of Wood Science*, *49*, 531–537.

Bai, W., Holbery, J., & Li, K. (2009). A technique for production of nanocrystalline cellulose with a narrow size distribution. *Cellulose*, *16*(3), 455–465.

Beck-Candanedo, S., Roman, M., & Gray, D. G. (2005). Effect of reaction conditions on the properties and behavior of wood cellulose nanocrystal suspensions. *Biomacromolecules*, *6*(2), 1048–1054.

Bondeson, D., Mathew, A., & Oksman, K. (2006). Optimization of the isolation of nanocrystals from microcrystalline cellulose by acid hydrolysis. *Cellulose*, *13*(2), 171–180.

Camarero Espinosa, S., Kuhnt, T., Foster, E. J., & Weder, C. (2013). Isolation of thermally stable cellulose nanocrystals by phosphoric acid hydrolysis. *Biomacromolecules*, *14*(4), 1223–1230.

Chum, H. L., Johnson, D. K., Black, S., Baker, J., Grohmann, K., Sarkanen, K. V., et al. (1988). Organosolv pretreatment for enzymatic-hydrolysis of poplars. 1. Enzyme hydrolysis of cellulosic residues. *Biotechnology and Bioengineering*, *31*(7), 643–649.

Dong, S., & Roman, M. (Eds.). (2012). *243rd ACS National Meeting & Exposition*. San Diego, CA, United States, March 25–29, 2012 (CELL-170),. American Chemical Society.

Dong, X., Revol, J.-F. O., & Gray, G. D. (1998). Effect of microcrystallite preparation conditions on the formation of colloid crystals of cellulose. *Cellulose*, *5*, 19–32.

Eichhorn, S. J. (2011). Cellulose nanowhiskers: Promising materials for advanced applications. *Soft Matter*, *7*(2), 303.

Elazzouzi-Hafraoui, S., Nishiyama, Y., Putaux, J.-L., Heux, L., Dubreuil, F., & Rochas, C. (2008). The shape and size distribution of crystalline nanoparticles prepared by acid hydrolysis of native cellulose. *Biomacromolecules*, *9*(1), 57–65.

Fan, J.-s., & Li, Y.-h. (2012). Maximizing the yield of nanocrystalline cellulose from cotton pulp fiber. *Carbohydrate Polymers*, *88*(4), 1184–1188.

Fink, H.-P., Hofmann, D., & Philipp, B. (1995). Some aspects of lateral chain order in cellulosics from X-ray scattering. *Cellulose*, *2*, 51–70.

Garvey, C. J., Parker, I. H., & Simon, G. P. (2005). On the interpretation of X-ray diffraction powder patterns in terms of the nanostructure of cellulose I fibres. *Macromolecular Chemistry and Physics*, http://dx.doi.org/10.1002/macp.200500008

George, J., Ramana, K. V., Bawa, A. S., & Siddaramaiah. (2011). Bacterial cellulose nanocrystals exhibiting high thermal stability and their polymer nanocomposites. *International Journal of Biology Macromolecules*, *48*(1), 50–57.

Guinier, A. (1963). *X-ray diffraction in crystals, imperfect crystals and amorphous bodies (a series of books in physics)*. San Francisco: W.H. Freeman.

Habibi, Y. (2014). Key advances in the chemical modification of nanocelluloses. *Chemical Society Reviews*, http://dx.doi.org/10.1039/c3cs60204d

Hamad, W. Y., & Hu, T. Q. (2010). Structure-process-yield interrelations in nanocrystalline cellulose extraction. *The Canadian Journal of Chemical Engineering*, *88*(3), 392–402.

Hermans, P. (1950). X-ray investigations on the crystallinity of cellulose. *Laboratory for Cellulose Research*, *68*, 25–29.

Herrera, M., Mathew, A., & Oksman, K. (2012). Comparison of cellulose nanowhiskers extracted from industrial bio-residue and commercial microcrystalline cellulose. *Materials Letters*, *71*, 28–31.

Hu, Y., Tang, L., Lu, Q., Wang, S., Chen, X., & Huang, B. (2014). Preparation of cellulose nanocrystals and carboxylated cellulose nanocrystals from borer powder of bamboo. *Cellulose*, http://dx.doi.org/10.1007/s10570-014-0236-0

Jiang, F., Esker, A. R., & Roman, M. (2010). Acid-catalyzed and solvolytic desulfation of H_2SO_4-hydrolyzed cellulose nanocrystals. *Langmuir*, *26*(23), 17919–17925.

Landry, V., Alemdar, A., & Blancher, P. (2010). Nanocrystalline cellulose: Morphological, physical, and mechanical properties. *Forest Products Journal*, *61*(2), 104–112.

Lazko, J., Sénéchal, T., Landercy, N., Dangreau, L., Raquez, J.-M., & Dubois, P. (2014). Well defined thermostable cellulose nanocrystals via two-step ionic liquid swelling-hydrolysis extraction. *Cellulose*, http://dx.doi.org/10.1007/s10570-014-0417-x

Leppänen, K., Andersson, S., Torkkeli, M., Knaapila, M., Kotelnikova, N., & Serimaa, R. (2009). Structure of cellulose and microcrystalline cellulose from various wood species, cotton and flax studied by X-ray scattering. *Cellulose*, *16*(6), 999–1015.

Leung, A. C. W., Hrapovic, S., Lam, E., Liu, Y., Male, K. B., Mahmoud, K. A., et al. (2011). Characteristics and properties of carboxylated cellulose nanocrystals prepared from a novel one-step procedure. *Small*, doi:10.1002/smll.201001715.

Li, C., & Zhao, Z. K. (2007). Efficient acid-catalyzed hydrolysis of cellulose in ionic liquid. *Advanced Synthesis & Catalysis*, *349*(11–12), 1847–1850.

Li, W., Yue, J., & Liu, S. (2012). Preparation of nanocrystalline cellulose via ultrasound and its reinforcement capability for poly (vinyl alcohol) composites. *Ultrasonics Sonochemistry*, *19*(3), 479–485.

Lin, C. H., Conner, A. H., & Hill, C. G. (1991). The heterogeneous character of the dilute acid hydrolysis of crystalline cellulose. II. Hydrolysis in sulfuric acid. *Journal of Applied Polymer Science*, *42*, 417–426.

Liu, Y., Wang, H., Yu, G., Yu, Q., Li, B., & Mu, X. (2014). A novel approach for the preparation of nanocrystalline cellulose by using phosphotungstic acid. *Carbohydrate Polymers*, http://dx.doi.org/10.1016/j.carbpol.2014.04.040

Magalhaes, W., Cao, X., & Lucia, A. L. (2009). Cellulose nanocrystals/cellulose core-in-shell nanocomposite assemblies. *Langmuir*, *25*(22), 13250–13257.

Majdanac, L. D., Poleti, D., & Teodorovic, M. J. (1991). Determination of the crystallinity of cellulose samples by X-ray diffraction. *Acta Polymerica*, *42*, 351–357.

Man, Z., Muhammad, N., Sarwono, A., Bustam, M. A., Kumar, M. V., & Rafiq, S. (2011). Preparation of cellulose nanocrystals using an ionic liquid. *Journal of Polymers and the Environment*, *19*(3), 726–731.

Mao, J., Osorio-Madrazo, A., & Laborie, M.-P. (2013). Preparation of cellulose I nanowhiskers with a mildly acidic aqueous ionic liquid: Reaction efficiency and whiskers attributes. *Cellulose*, *20*(4), 1829–1840.

Mathew, A. P., & Dufresne, A. (2002). Morphological investigation of nanocomposites from sorbitol plasticized starch and tunicin whiskers. *Biomacromolecules*, *3*(3), 609–617.

Moon, R. J., Martini, A., Nairn, J., Simonsen, J., & Youngblood, J. (2011). Cellulose nanomaterials review: Structure, properties and nanocomposites. *Chemical Society Reviews*, *40*(7), 3941–3994.

Nelson, M. L., & O'Connor, R. (1964). Relation of certain infrared bands to cellulose crystallinity and crystal latticed type. Part I. Spectra of lattice types I, II, III and of amorphous cellulose. *Journal of Applied Polymer Science*, *8*, 1311–1324.

Nishino, T., Takano, K., & Nakamae, K. (1995). Elastic modulus of the crystalline regions of cellulose polymorphs. *Journal of Polymer Science Part B: Polymer Physics*, *33*, 1647–1651.

Nishiyama, Y., Langan, P., & Chanzy, H. (2002). Crystal structure and hydrogen-bonding system in cellulose iβ from synchrotron X-ray and neutron fiber diffraction. *Journal of the American Chemical Society*, *124*(31), 9074–9082.

Nishiyama, Y., Sugiyama, J., Chanzy, H., & Langan, P. (2003). Crystal structure and hydrogen bonding system in cellulose iα from synchrotron X-ray and neutron fiber diffraction. *Journal of the American Chemical Society*, *125*(47), 14300–14306.

Oh, S. Y., Yoo, D. I., Shin, Y., Kim, H. C., Kim, H. Y., Chung, Y. S., et al. (2005). Crystalline structure analysis of cellulose treated with sodium hydroxide and carbon dioxide by means of X-ray diffraction and FTIR spectroscopy. *Carbohydrate Research*, *340*(15), 2376–2391.

Overend, B., Chornet, E., & Gascoigne, J. (1987). Fractionation of lignocellulosics by steam-aqueous pretreatments [and discussion]. *Philosophical Transactions of the Royal Society*, *321*, 523–536.

Peterlin, A., & Zachmann, H. G. (1971). Amorphous surface layers in polyethylene single crystals. *Journal of Polymer Science Part C: Polymer Symposia*, *34*, 11–20.

Revol, J., Dietrich, A., & Goring, D. (1987). Effect of mercerization on the crystallite size and crystallinity index in cellulose from different sources. *The Canadian Journal of Chemical Engineering*, *65*, 1724.

Rusli, R., Shanmuganathan, K., Rowan, S. J., Weder, C., & Eichhorn, S. J. (2011). Stress transfer in cellulose nanowhisker composites – Influence of whisker aspect ratio and surface charge. *Biomacromolecules*, *12*(4), 1363–1369.

Sakurada, I., Nukushina, Y., & Ito, T. (1962). Experimental determination of elastic modulus of crystalline regions in printed polymers. *Journal of Polymer Science*, *57*(165), 651–660.

Segal, L., Creely, J. J., Martin, A. E., & Conrad, C. M. (1959). An empirical method for estimating the degree of crystallinity of native cellulose using the X-ray diffractometer. *Textile Research Journal*, http://dx.doi.org/10.1177/004051755902901003

Strobl, G. R. (2007). *The physics of polymers: Concepts for understanding their structures and behavior; with 2 tables* (3rd ed.). Berlin, Heidelberg [u.a.]: Springer.

Sturcova, A., Davies, G. R., & Eichhorn, S. J. (2005). Elastic modulus and stress-transfer properties of tunicate cellulose whiskers. *Biomacromolecules*, *6*(2), 1055–1061.

Tang, L., Huang, B., Lu, Q., Wang, S., Ou, W., Lin, W., et al. (2013). Ultrasonication-assisted manufacture of cellulose nanocrystals esterified with acetic acid. *Bioresource Technology*, http://dx.doi.org/10.1016/j.biortech.2012.09.133

Tang, L., Huang, B., Yang, N., Li, T., Lu, Q., Lin, W., et al. (2013). Organic solvent-free and efficient manufacture of functionalized cellulose nanocrystals via one-pot tandem reactions. *Green Chemistry*, http://dx.doi.org/10.1039/c3gc40965a

Tang, L.-r., Huang, B., Ou, W., Chen, X.-r., & Chen, Y.-d. (2011). Manufacture of cellulose nanocrystals by cation exchange resin-catalyzed hydrolysis of cellulose. *Bioresource Technology*, http://dx.doi.org/10.1016/j.biortech.2011.09.070

Tang, Y., Yang, S., Zhang, N., & Zhang, J. (2014). Preparation and characterization of nanocrystalline cellulose via low-intensity ultrasonic-assisted sulfuric acid hydrolysis. *Cellulose*, doi:10.1007/s10570-013-0158-2.

Thygesen, A., Oddershede, J., Lilholt, H., Thomsen, A. B., & Ståhl, K. (2005). On the determination of crystallinity and cellulose content in plant fibres. *Cellulose*, http://dx.doi.org/10.1007/s10570-005-9001-8

Wang, N., Ding, E., & Cheng, R. (2007). Thermal degradation behaviors of spherical cellulose nanocrystals with sulfate groups. *Polymer*, *48*(12), 3486–3493.

Wegner, T. H., & Jones, P. E. (2006). Advancing cellulose-based nanotechnology. *Cellulose*, *13*, 115–118.

Yu, H., Qin, Z., Liang, B., Liu, N., Zhou, Z., & Chen, L. (2013). Facile extraction of thermally stable cellulose nanocrystals with a high yield of 93% through hydrochloric acid hydrolysis under hydrothermal conditions. *Journal of Materials Chemistry A*, http://dx.doi.org/10.1039/c3ta01150j

Zhang, J., Zhang, J., Lin, L., Chen, T., Zhang, J., Liu, S., et al. (2009). Dissolution of microcrystalline cellulose in phosphoric acid – Molecular changes and kinetics. *Molecules*, *14*(12), 5027–5041.

Zhang, K., Brendler, E., & Fischer, S. (2010). FT Raman investigation of sodium cellulose sulfate. *Cellulose*, http://dx.doi.org/10.1007/s10570-009-9375-0

Zhao, X., Liu, Z., & Zhang, S. (2012). Optimization of microwave-assisted acid hydrolysis preparation of reed pulp nanocrystalline cellulose. *Guangdong Huagong*, *39*(10), 3–4.